Original article
DOI: https://doi.org/10.18721/JPM.18410

MODIFICATION OF MORPHOLOGY OF THIN NICKEL AND ZIRCONIUM FILMS ON NATURALLY OXIDIZED SILICON SUBSTRATES BY ANNEALING IN VACUUM

V. T. A. Nguyen, P. G. Gabdullin, A. V. Arkhipov✉

Peter the Great St. Petersburg Polytechnic University, St. Petersburg, Russia

✉ arkhipov@rphf.spbstu.ru

Abstract. The article presents a technique for fabricating nickel island films on oxidized silicon substrates by thermal dewetting of continuous coatings. First, continuous nickel films 5 nm thick were deposited by magnetron sputtering. Then, without exposure to the atmosphere, the coatings were annealed in a vacuum at 450°C for 15–180 min. As a result, the formation of isolated metal islands was on the substrate with transverse dimensions from units to tens of nanometers, depending on the annealing time. The electrical and thermoelectrical characteristics of the produced island films were determined. Attempts to prepare zirconium island films using the same technique were unsuccessful as the technically available annealing temperature of 650 °C proved insufficient for dewetting of coatings made of this material.

Keywords: thin film, island film, nanoparticle, film dewetting, Ni, Zr, thermoelectrical coefficient

Citation: Nguyen V. T. A., Gabdullin P. G., Arkhipov A. V., Modification of morphology of thin nickel and zirconium films on naturally oxidized silicon substrates by annealing in vacuum, St. Petersburg State Polytechnical University Journal. Physics and Mathematics. 18 (4) (2025) 139–150. DOI: https://doi.org/10.18721/JPM.18410

Научная статья
УДК 539.216.2
DOI: https://doi.org/10.18721/JPM.18410

ТРАНСФОРМАЦИЯ МОРФОЛОГИИ ТОНКИХ ПЛЕНОК НИКЕЛЯ И ЦИРКОНИЯ НА ЕСТЕСТВЕННО ОКИСЛЕННЫХ КРЕМНИЕВЫХ ПОДЛОЖКАХ ПРИ ОТЖИГЕ В ВАКУУМЕ

В. Т. А. Нгуен, П. Г. Габдуллин, А. В. Архипов✉

Санкт-Петербургский политехнический университет Петра Великого, Санкт-Петербург, Россия

✉arkhipov@rphf.spbstu.ru

Аннотация. В статье представлена технология получения островковых пленок никеля на поверхности окисленных кремниевых подложек методом термического деветтинга (агломерации) сплошных покрытий. Вначале сплошные пленки никеля толщиной 5 нм наносились на подложки методом магнетронного напыления. Затем, без выноса на атмосферу, производился отжиг покрытий в вакууме при температуре 450 °C продолжительностью от 15 мин до 3 ч. Результатом этого было формирование на подложке изолированных металлических островков с поперечными размерами от единиц до десятков нанометров, в зависимости от времени отжига. Были определены электрические и термоэлектрические характеристики полученных островковых пленок. Попытки приготовления островковых пленок циркония с использованием той же методики не принесли успеха, так как технически реализуемая температура отжига 650 °C оказалась недостаточной для агломерации покрытий из этого материала.

Ключевые слова: тонкая пленка, островковая пленка, наночастица, деветтинг пленок, никель, термоэлектрический коэффициент

Ссылка для цитирования: Нгуен В. Т. А., Габдуллин П. Г., Архипов А. В. Трансформация морфологии тонких пленок никеля и циркония на естественно окисленных кремниевых подложках при отжиге в вакууме // Научно-технические ведомости СПбГПУ. Физико-математические науки. 2025. Т. 18. № 4. С. 139–150. DOI: https://doi.org/10.18721/JPM.18410

Introduction

Metal nanoparticles and clusters are finding new applications in engineering and medicine due to their unique properties [1–4]. Some of their well-known useful qualities include, for example, enhancing local optical frequency fields due to local plasmon resonance. Other properties of nanoparticles have been studied to a lesser extent, in particular, the capability for low-field electron emission [5–10], as well as high thermoelectric performance [11–14].

An island film of a conducting material on a poorly conducting substrate can be classified as a disordered array of nanoparticles exhibiting many properties inherent to such structures. This is confirmed by the results of the experimental studies conducted at Peter the Great St. Petersburg Polytechnic University on the emission properties of carbon and metal island films on silicon substrates, detecting low-field electron emission in such films [15–18]. However, the metal films (Mo, Zr, Ni) used in [17, 18] were initially prepared as continuous, acquiring an island structure during the experiments due to emission-related factors. This makes it difficult to interpret the results.

The goal of this study was to develop a technology for producing island film samples of varying morphology to continue the experiments. Zirconium and nickel were chosen as coating materials, as the films based on them exhibited electron emission in [17, 18]. The advantage of zirconium and nickel over molybdenum, whose films exhibit the best emission capability, is a lower melting point, which simplifies the technology for their heat treatment. The same substrates were used for comparison with the data in [15–18]: KDB10 silicon wafers with a preserved natural oxide layer.

The approach to obtaining island films of the chosen metals relied on thermal dewetting: continuous thin metal films agglomerate when deposited onto non-wettable dielectric substrates, transforming into nanoscale droplets. The term «solid-state dewetting» is commonly used in the English-language literature for such a process [4, 19–24], since it does not require melting of the coating material. Dewetting is influenced by surface tension forces and can be induced, in particular, by heating such films in vacuum or in an inert (or reducing) atmosphere, while the temperature required is typically significantly (by hundreds of degrees) lower than the melting point of the corresponding metal.

Aside from investigating the emission properties of island coatings (which falls outside the scope of this paper), we planned to conduct initial experiments to study the thermoelectric characteristics of metal island contacts with a substrate [25]. The objective was both to verify the validity of the thermoelectric model of electron emission facilitated by island films (proposed in [18, 26]) and to explore their potential applications in efficient thermoelectric converters [27].

Methods and materials

Thermal dewetting for manufacturing of island coatings consists of two sequential stages:
continuous film is deposited on the surface of the substrate;
this film is transformed into island coating by annealing.

Both stages were carried out in a HEX growth chamber (by Mantis Deposition, UK) without exposure to the atmosphere, making it possible to avoid oxidation of continuous thin films before annealing.

Continuous nickel or zirconium films with a thickness of 5 nm were deposited on substrates by magnetron sputtering of targets made of nickel-vanadium alloy (NiV) or pure zirconium (Zr), respectively. A two-inch magnetron which is part of the HEX system was used for this purpose. The discharge voltage and current were 450 V and 250 mA; the process was carried out at a buffer gas (argon) pressure of 10^{-3}mbar and room temperature of the substrates. The film growth rate was 0.3 Å/s. It was determined by a quartz crystal microbalance and additionally monitored by the topography profiles of mechanically damaged reference coating samples.

Targets made of non-magnetic NiV alloy (at a vanadium concentration of 7 wt.%) were used for depositing nickel films due to low efficiency of magnetron sputtering for ferromagnetics. Special EDS measurements were carried out using a scanning electron microscope to evaluate the vanadium contents in the deposited coatings. Due to vanadium's low sputtering yield, its content in the films turned out to be insignificant, below the sensitivity threshold of the method, which can be estimated as 0.5–1.0 wt.% for such thin films. We refer to such films as nickel films, although we understand that they are not pure nickel, but contain a small vanadium impurity (difficult to determine and likely distributed non-uniformly).

Coating samples were formed on substrates approximately 10×10 mm in size, cut from KDB-10 silicon wafers with a (100) surface orientation. The natural oxide layer was not removed from the surface of the substrates. Organic impurities were removed by mechanical and ultrasonic treatment in acetone with further washing with isopropyl alcohol and distilled water.

The deposited nickel coatings were annealed in vacuum at 450 °C, the zirconium coatings were annealed at 550–650 °C. The annealing time varied from 15 to 180 min. Pumping of the growth chamber allowed to limit the pressure of residual gases at a level not worse than 10^{-5} Torr.

The topography of the prepared samples was studied using a NanoDST atomic force microscope (AFM) (Pacific Nanotechnology, USA). The measurements were carried out under ambient conditions in tapping mode with NSG10 probes (NT-MDT, Russia). The same microscope was used for thermoelectric measurements. In this case, a Peltier device was mounted on the positioning stage of the microscope, allowing to adjust the temperature of the sample to in the range of 0–80 °C. The sample was electrically isolated from the positioning stage and its potential relative to the microscope probe (electrically connected to the frame) was measured with a B7-72 voltmeter (MNIPI, Belarus). The probe was brought into contact with the sample with the AFM feedback loop either disabled or enabled; in the second case, the microscope operated in contact mode (vibration-free). DEP01 probes (NT-MDT, Russia) with a soft cantilever (2.8 N/m) and a tip made of highly conductive boron-doped diamond were used for thermoelectric measurements. This probe was selected based on the results of preliminary tests with several types of probes.

The electrical characteristics of the films were measured using an L2-100TECO curve tracer (Testpribor, Russia). Measurements of the current–voltage characteristics were carried out both in-plane and cross-plane relative to the coating. The probes were placed at a distance of approximately 2 mm from each other for measurements of the film resistance. When the contact resistance of the film with the substrate was measured, one of the probes was placed on the selected segment of the film, and the second one was placed opposite the first one on the other side of the substrate.

Experimental results and discussion

Zirconium films. The results for annealing zirconium films in vacuum are represented in Fig. 1 by images of the surface topography of the samples before and after annealing of different durations. Clearly, there are no obvious signs of thermal agglomeration on them under these conditions and the coating remains fairly uniform. The total height of the relief, as before annealing, only slightly exceeds 2 nm.

An exception is the image in Fig. 1,*c* for a coating exposed at a maximum available temperature of 650 °C for one hour. Elongated crystallites are discernible in it, which can be regarded as a sign of the emergent agglomeration of the coating. We reached this conclusion based on the findings in [28], where emission-related factors were found to induce the formation of nanowires during agglomeration of zirconium films. These structures were markedly different in shape from the rounded nanoislands produced by agglomeration of molybdenum films induced by the same factors.

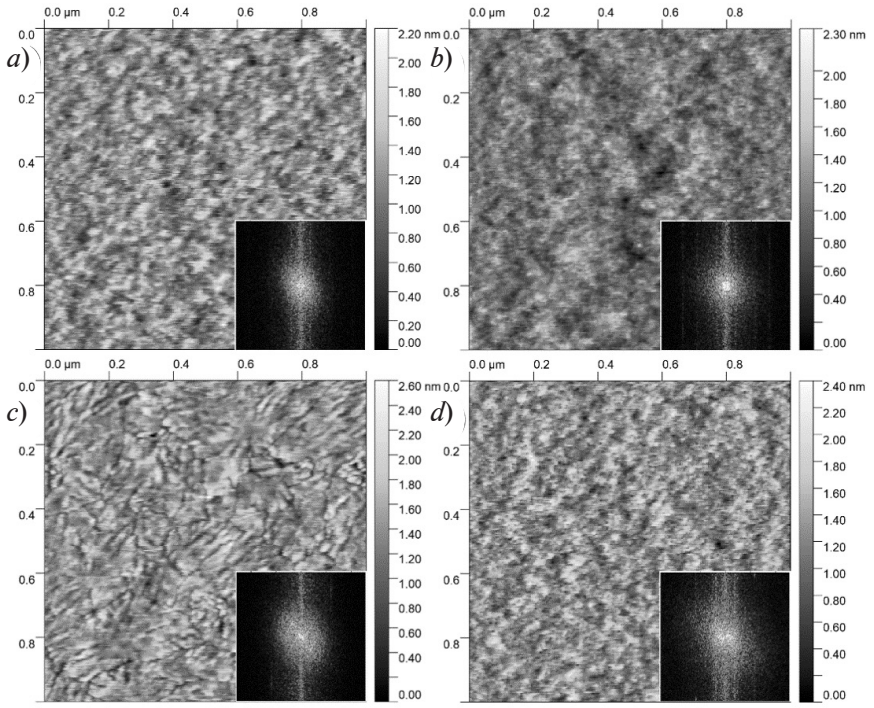

Fig. 1. AFM images of surface topography for 5-nm-thick zirconium films: freshly prepared (*a*); after annealing at 550 °C (60 min) (*b*); at 650 °C (60 min) (*c*); at 650 °C (120 min) (*d*)
Insets: 2D Fourier spectra of AFM images

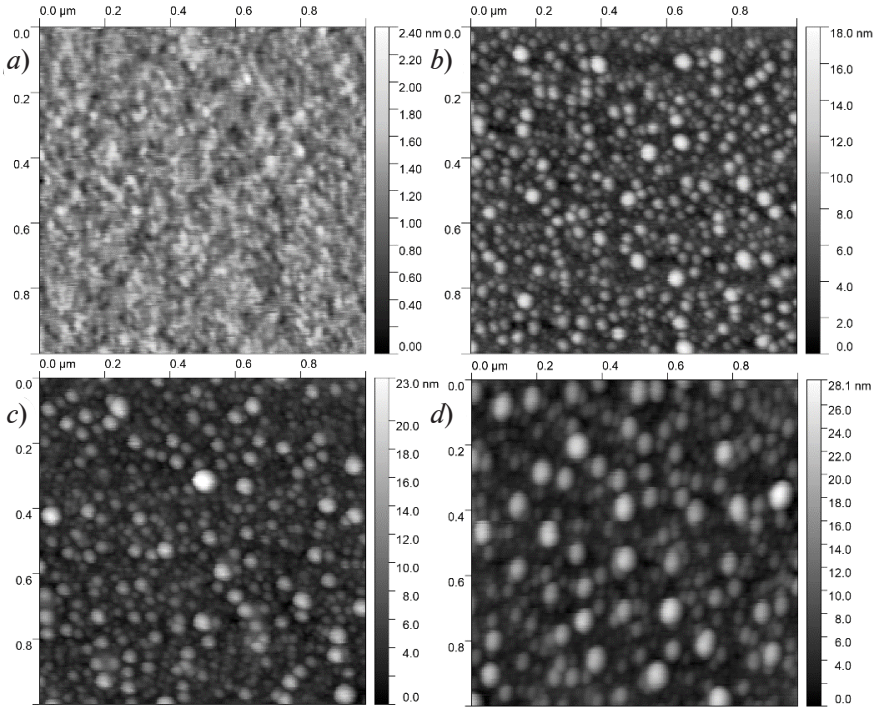

Fig. 2. AFM images for topography of nickel films with initial thickness of 5 nm: freshly prepared films (*a*); after annealing in vacuum at 450 °C for 30 min (*b*), 60 min (*c*) and 120 min (*d*)

Admittedly however, similar signs pointing to the onset of the morphological transformation are not observed in Fig. 1,*d*, obtained for a coating subjected to heat treatment at the same temperature (650 °C) for twice as long (2 hours). This may indicate a significant variation in the surface properties of the naturally oxidized substrates used, affecting the stability of the films. This variation was noted earlier based on the results of experiments with films of metals [17, 18] and carbon [15, 16].

To identify the finer details of AFM images that are not visually observable, two-dimensional Fourier analysis was performed by applying the 2D FFT function of the Gwyddion 2.62 package to the images. Prior to analysis, all raw data underwent identical digital processing aimed to minimize measurement artifacts, such as row misalignment caused by tip instability. The obtained Fourier spectra of the film topography are shown in the insets in Fig. 1. A certain broadening can be detected with increasing annealing temperature and time, reflecting an increase in image granularity on a spatial scale of about 10 nm. Such broadening may signal a reorganization of the film's nanostructure that begins upon annealing.

Nickel films. Annealing at 450 °C proved sufficient to transform the structure of a 5-nm-thick continuous nickel coating to an island one. Fig. 2,*a* shows a typical AFM image for the surface of a continuous nickel film after magnetron sputtering. Figs. 2, *b*–*d* represent the topography of the samples after heating in vacuum for 30, 60, and 120 minutes. Evidently, agglomeration of the film with the formation of rounded islands occurs.

Fig. 3 shows the results of statistical processing for a series of AFM images of the film topography. Fig. 3,*a* shows the dependences on the annealing time for standardized roughness parameters of the film surface, calculated using the Gwyddion package for both maximum and median

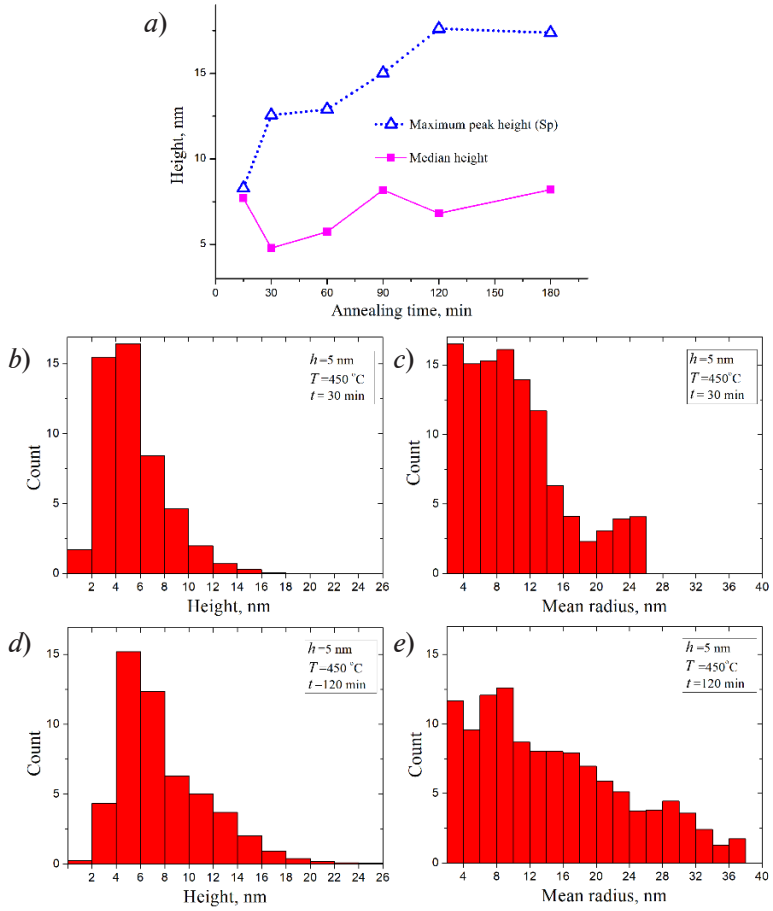

Fig. 3. AFM images for topography of Ni films with initial thickness of 5 nm: dependences of surface roughness parameters on annealing time at 450 °C (*a*) (symbols ■ and △ correspond to median and maximum height); histograms of island height (*b*, *d*) and radius (*c*, *e*), for coatings after annealing for 30 min (*b*, *c*) and 2 h (*d*, *e*)

heights of the protruding islands. The graph of the maximum peak height (i.e., the height of the largest islands measured from the median plane) shows a monotonic increase in this parameter with increasing annealing time; its highest value is close to 20 nm. The median height remains in the range from 5 to 8 nm, which approximately corresponds to the initial coating thickness.

Fig. 3, *b*, and *d* shows histograms for the heights of individual islands, Fig. 3, *c*, and *e* shows histograms for their lateral dimensions. These data correspond to films heated for 30 and 120 minutes. The longer annealing time corresponds to wider distributions of these parameters, as well as an approximately 50% increase in the maximum lateral sizes of the islands as the coatings are annealed, which is typical for thermal agglomeration [19]. After two hours of annealing, the radius of the large islands reached 35–40 nm at a height of 20–25 nm (see Fig. 3, *d*, *e*).

Fig. 4 shows the measurement results for the surface conductivity of coatings, exhibiting a qualitative change in the nature of their conductivity after annealing. The as-deposited films are continuous despite their small mean thickness, as evidenced by the ohmic (linear) behavior of their current–voltage characteristic and high electrical conductivity with small variance of electrical parameters (Fig. 4,*a*). The current–voltage characteristics of annealed coatings (Fig. 4,*b*) are nonlinear, changing significantly when the contacts are moved along the surface; considerably high voltages are required to obtain the given current value in this case. Here the natural explanation is that the continuous current paths in the metal film are interrupted as it breaks up into islands. The films were not photoconductive either before or after annealing: illumination with red light from a semiconductor laser did not lead to a change in the current–voltage characteristics (as marked by the 'laser on/off' labels in the legends to the graphs in Fig. 4).

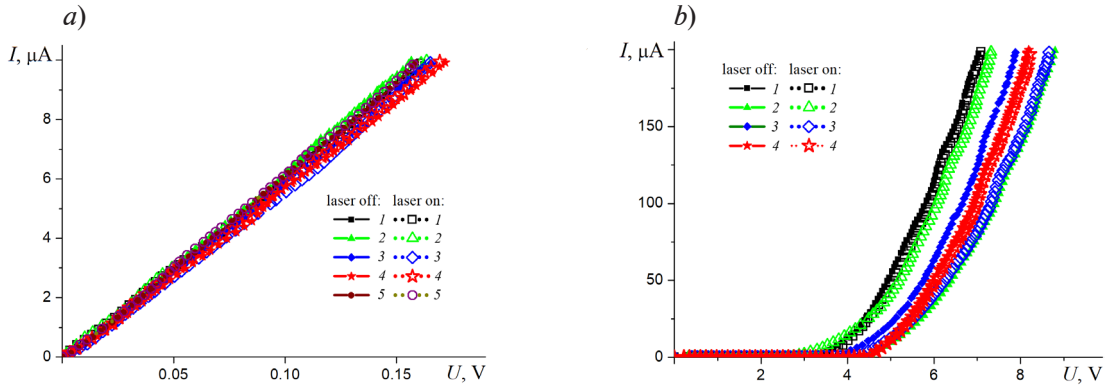

Fig. 4. Measurements of conductivity along unannealed (*a*) and annealed (in vacuum at 450 °C for 60 min) (*b*) Ni coatings
Curves with different numbers correspond to different pairs of contact points on the same sample

Fig. 5,*a* illustrates the change in the conductivity characteristics along the surface of nickel coating samples with increasing annealing time. Notably, the current–voltage characteristics are nonlinear even with a minimum annealing time (15 min), clearly reflecting the fact that the agglomeration of films is already completed by this time. The nonlinear behavior of the current–voltage characteristics in the island films can be attributed to both in-plane conduction via charge carrier tunneling between metal islands and to cross-plane conduction. In the second case, carriers have to overcome the interface between the substrate and the coating (partially consisting of a preserved silicon dioxide layer) twice. Ultimately, this indirect evidence supports the latter hypothesis. One of the signs is the smooth and reproducible shape of the current–voltage characteristics in Figs. 4,*b* and 5,*a*: the flow of tunneling current through island films is usually accompanied by their electroforming [29], manifesting as instability and hysteresis of the current dependences. Another sign is the relatively slow and monotonic evolution of the current–voltage characteristics with increasing annealing time (accounting for the above-mentioned variance of substrate properties). If tunneling conduction were dominant, a much sharper change might be expected for the in-plane conductivity as the gaps between the islands widen.

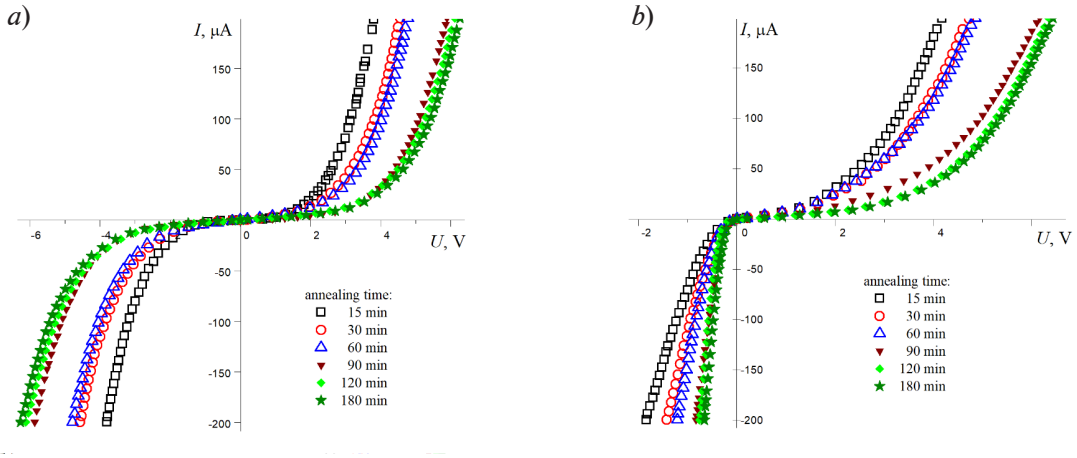

Fig. 5. In-plane (*a*) and cross-plane (*b*) current–voltage characteristics for nickel film samples with a thickness of 5 nm after annealing at 450 °C for different durations

Further evidence for current flow through the substrate during in-plane $I-V$ measurements comes from the shape of the characteristics measured in the cross-plane direction, between a point on the film and an ohmic contact on the back side of the silicon wafer. Such current–voltage characteristics are shown in Fig. 5,*b*. Their shape is asymmetrical, and the degree of asymmetry increases with increasing annealing time. One of the branches (the right one) of each of the above dependences is similar in shape and quantitative parameters to the symmetrical branches of the in-plane $I-V$ curves for the corresponding sample (see Fig. 5,*a*). *The* other branch (the left one) is characterized by a higher current. Such patterns can be easily interpreted if we assume that the islands in annealed coatings are separated from the substrate by Schottky contacts whose $I-V$ curves are close to those shown in Fig. 5,*b*. The current path includes two such contacts connected back-to-back for in-plane measurements (see Fig. 5,*a*). The resulting $I-V$ curve is symmetric, with its branches corresponding to the reverse branch of a Schottky diode. The dependence of the shape of the $I-V$ curve on the annealing time of the coating can be determined to a decrease in the effective contact area as the islands in the coating are isolated from each other.

Coating and substrate samples were then used in experiments to determine the thermoelectric properties of their nanocontacts with the probe of the atomic force microscope. The measured values of the Seebeck coefficient S for the nanocontact probe with an unannealed film and a substrate without a metal coating were low (not exceeding approximately 4 μV/K). Values of the Seebeck coefficient of this order are typical for metals, although the tip of the AFM probe used was made of semiconducting doped diamond. The values of the Seebeck coefficient for semiconductors are typically 1–2 orders of magnitude higher. This result confirms a general pattern known from the literature (see, for example, [30]): suppression of the thermoelectric effect in micro- and nanocontacts.

On the other hand, experiments with a nickel island film obtained by annealing a 5-nm-thick continuous film at 450 °C for 60 minutes (see Fig. 1,*c*) yielded a qualitatively different result. When this sample, heated to 65 °C, contacted the probe with the ambient temperature of 20 °C, a thermoelectric potential difference up to 3.4 mV was recorded, which corresponds to the Seebeck coefficient $S \approx 75$ μV/K. This exceeds the typical values of S for metals and corresponds in order of magnitude to the typical values for doped semiconductors. Therefore, no significant suppression of the thermoelectric effect occurred in this case. This may be due to the size effects in nickel nanoislands or to the peculiarities of the interface between the island and the substrate. This interface has a relatively low electrical conductivity (due to the presence of an oxide layer and a Schottky barrier) while maintaining high-quality acoustic contact. The lateral dimension of the interface is about 20 nm, which is significantly larger than the area of the contact between the AFM probe and a flat film or substrate. All of this facilitates the efficient conversion of heat flux from electronic (in the island) to phononic (in the substrate) form and vice versa. The fundamental possibility of effective thermoelectric conversion under such conditions was analyzed in a recent theoretical paper [27].

Conclusion

The objective of this study was to develop a technology for producing nickel island films on oxidized KDB-10 silicon wafers, which was achieved by means of thermal agglomeration (dewetting). For this purpose, it was sufficient to heat the continuous coatings with a thickness of 5 nm in vacuum at 450 °C. The process parameters reported in the literature could not be adopted without additional verification, as it is known that the agglomeration temperature of thin films depends not only on the coating material but also on its thickness [24], presence of impurities [31], and substrate material [32]. Considering all of these factors, the conditions closest to our experiments with nickel appear to be those in [3], studying the agglomeration of initially continuous 3.0-nm-thick nickel films deposited on Si(100) wafers with a 4.5-nm oxide layer. It is pointed out in [3] that the continuous film structure began to disintegrate (i.e., holes appeared) at an annealing temperature as low as 280 °C; however, the heating to 450 °C was required for isolated islands to form, which is in good agreement with the results of our experiments.

The lateral dimensions (radii) of the nickel islands obtained in our experiments ranged from a few units to 35–40 nm. Electrical characterization of the films showed that the islands are weakly coupled: the electrical conductivity along the coating is primarily governed by currents flowing through the substrate and the island/substrate interfaces. Both the morphological and electrical parameters of the coatings could be modified by varying the annealing time. Applying the same technique to zirconium films of the same average thickness (5 nm) revealed that annealing at 650 °C was insufficient to transform their structure into an island morphology.

Initial AFM measurements of the thermoelectric parameters of nickel nanoisland films show potential for further research into these structures to enhance the thermoelectric performance.

REFERENCES

1. **Daniel M.-C., Astruc D.,** Gold nanoparticles: Assembly, supramolecular chemistry, quantum-size-related properties, and applications toward biology, catalysis, and nanotechnology, Chem. Rev. 104 (1) (2004) 293–346.

2. **Yeh Y.-C., Creran B., Rotello V. M.,** Gold nanoparticles: preparation, properties, and applications in bionanotechnology, Nanoscale. 4 (6) (2012) 1871–1880.

3. **Dufourcq J., Mur P., Gordon M.J., et al.,** Metallic nano-crystals for flash memories, Mater. Sci. Eng. C. 27 (5–8) (2007) 1496–1499.

4. **Kitsyuk E. P., Vasilevskaya Yu. O., Volovlikova O. V., et al.,** Catalytic particles formation from thin nickel films for the synthesis of multi-walled carbon nanotubes, Carbon. 229 (11) (2024) 119509.

5. **Filip V., Filip L.D., Wong H.,** Review on peculiar issues of field emission in vacuum nanoelectronic devices, Solid State Electron. 138 (Dec) (2017) 3–15.

6. **Filip L. D., Palumbo M., Carey J. D., Silva S. R. P.,** Two-step electron tunneling from confined electronic states in a nanoparticle, Phys. Rev. B. 79 (24) (2009) 245429.

7. **Gloskovskii A., Valdaitsev D.A., Cinchetti M., et al.,** Electron emission from films of Ag and Au nanoparticles excited by a femtosecond pump-probe laser, Phys. Rev. B. 77 (19) (2008) 195427.

8. **Fursey G., Konorov P., Pavlov B., Yafyasov A.,** Dimensional quantization and the resonance concept of the low-threshold field emission, Electronics. 4 (4) (2015) 1101–1108.

9. **Davidovich M. V., Yafarov R. K.,** Pulsed and static field emission VAC of carbon nanocluster structures: experiment and its interpretation, Tech. Phys. 64 (8) (2019) 1210–1220.

10. **Kleshch V. I., Porshyn V., Lützenkirchen-Hecht D., Obraztsov A. N.,** Coulomb blockade and quantum confinement in field electron emission from heterostructured nanotips, Phys. Rev. B. 102 (23) (2020) 235437.

11. **Bergfield J. P., Solis M. A., Stafford C. A.,** Giant thermoelectric effect from transmission supernodes, ACS Nano. 4 (9) (2010) 5314–5320.

12. **Dubi Y., Di Ventra M.,** Colloquium: Heat flow and thermoelectricity in atomic and molecular junctions, Rev. Mod. Phys. 83 (1) (2011) 131–155.

13. **Karlstrцm O., Linke H., Karlstrцm G., Wacker A.,** Increasing thermoelectric performance using coherent transport, Phys. Rev. B. 84 (11) (2011) 113415.

14. **Sadeghi H.,** Quantum and phonon interference-enhanced molecular-scale thermoelectricity, J. Phys. Chem. C. 123 (20) (2019) 12556–12562.

15. **Andronov A., Budylina E., Shkitun P., et al.,** Characterization of thin carbon films capable of low-field electron emission, J. Vac. Sci. Technol. B. 36 (2) (2018) 02C108.

16. **Gabdullin P., Zhurkin A., Osipov V., et al.,** Thin carbon films: correlation between morphology and field-emission capability, Diam. Relat. Mater. 105 (May) (2020) 107805.

17. **Bizyaev I. S., Gabdullin P. G., Gnuchev N. M., Arkhipov A. V.,** Low-field electron emission from thin films of metals, St. Petersburg State Polytechnical University Journal. Physics and Mathematics. 14 (1) (2021) 105–120.

18. **Bizyaev I., Gabdullin P., Chumak M., et al.,** Low-field electron emission capability of thin films on flat silicon substrates: Experiments with Mo and general model for refractory metals and carbon, Nanomater. 11 (12) (2021) 3350.

19. **Thompson C. V.,** Solid-state dewetting of thin films, Annu. Rev. Mater. Res. 42 (1) (2012) 399–434.

20. **Ruffino F., Grimaldi G.,** Controlled dewetting as fabrication and patterning strategy for metal nanostructures, Phys. Status Solidi A. 212 (8) (2015) 1662–1684.

21. **Niekiel F., Schweizer P., Kraschewski S.M., et al.,** The process of solid-state dewetting of Au thin films studied by in situ scanning transmission electron microscopy, Acta Mater. 90 (15 May) (2015) 118–132.

22. **Kovalenko O., Szaby S., Klinger L., Rabkin E.,** Solid state dewetting of polycrystalline Mo film on sapphire, Acta Mater. 139 (15 Oct) (2017) 51–61.

23. **Weil K. S., Mast E. S., Sprenkle V. L.,** Agglomeration behavior of solid nickel on polycrystalline barium titanate, Mater. Lett. 61 (28) (2007) 4993–4996.

24. **Alburquenque D., Del Canto M., Arenas C., et al.,** Dewetting of Ni thin films obtained by atomic layer deposition due to the thermal reduction process: Variation of the thicknesses, Thin Solid Films. 638 (30 Sept) (2017) 114–118.

25. **Trofimovich K. R., Gabdullin P. G., Arkhipov A. V.,** An experimental apparatus for studying the characteristics of thermoelectric effect in nanostructures, St. Petersburg State Polytechnical University Journal. Physics and Mathematics. 16 (4) (2023) 101–117 (in Russian).

26. **Arkhipov A. V., Eidelman E. D., Zhurkin A. M., et al.,** Low-field electron emission from carbon cluster films: combined thermoelectric/hot-electron model of the phenomenon, Fuller. Nanotub. Car. N. 28 (4) (2020) 286–294.

27. **Arkhipov A., Trofimovich K., Arkhipov N., Gabdullin P.** Phonon drag contribution to thermopower for a heated metal nanoisland on a semiconductor substrate, Nanomater. 14 (20) (2024) 1684.

28. **Bizyaev I. S., Karaseov P. A., Karabeshkin K. V., et al.,** Transformation of the structure of thin metal films upon activation of their ability to low-voltage electron emission // St. Petersburg State Polytechnical University Journal. Physics and Mathematics. 17 (2) (2024) 80–93 (in Russian).

29. **Fedorovich R. D., Naumovets A. G., Tomchuk P. M.,** Electron and light emission from island metal films and generation of hot electrons in nanoparticles, Phys. Rep. 328 (2–3) (2000) 73–179.

30. **Weber L., Lehr M., Gmelin E.,** Reduction of the thermopower in semiconducting point contacts, Phys. Rev. B. 46 (15) (1992) 9511–9514.

31. **Barda H., Rabkin E.,** Improving the thermal stability of nickel thin films on sapphire by a minor alloying addition of gold, Appl. Surf. Sci. 484 (1 Aug) (2019) 1070–1079.

32. **Nsimama P. D., Herz A., Wang D., Schaaf P.,** Influence of the substrate on the morphological evolution of gold thin films during solid-state dewetting, Appl. Surf. Sci. 388 (A) (2016) 475–482.

СПИСОК ЛИТЕРАТУРЫ

1. **Daniel M.-C., Astruc D.** Gold nanoparticles: Assembly, supramolecular chemistry, quantum-size-related properties, and applications toward biology, catalysis, and nanotechnology // Chemical Reviews. 2004. Vol. 104. No. 1. Pp. 293–346.

2. **Yeh Y.-C., Creran B., Rotello V. M.** Gold nanoparticles: preparation, properties, and applications in bionanotechnology // Nanoscale. 2012. Vol. 4. No. 6. Pp. 1871–1880.

3. **Dufourcq J., Mur P., Gordon M. J., Minoret S., Coppard R., Baron T**. Metallic nano-crystals for flash memories // Materials Science & Engineering C. 2007. Vol. 27. No. 5–8, Pp. 1496–1499.

4. **Kitsyuk E. P., Vasilevskaya Yu. O., Volovlikova O. V., Eganova E. M., Dudin A. A.** Catalytic particles formation from thin nickel films for the synthesis of multi-walled carbon nanotubes // Carbon. 2024. Vol. 229. No. 11. P. 119509.

5. **Filip V., Filip L. D., Wong H.** Review on peculiar issues of field emission in vacuum nanoelectronic devices // Solid State Electronics. 2017. Vol. 138. December. Pp. 3–15.

6. **Filip L. D., Palumbo M., Carey J. D., Silva S. R. P.** Two-step electron tunneling from confined electronic states in a nanoparticle // Physical Review B. 2009. Vol. 79. No. 24. P. 245429.

7. **Gloskovskii A., Valdaitsev D. A., Cinchetti M., et al.** Electron emission from films of Ag and Au nanoparticles excited by a femtosecond pump-probe laser // Physical Review B. 2008. Vol. 77. No. 19, P. 195427.

8. **Fursey G., Konorov P., Pavlov B., Yafyasov A.** Dimensional quantization and the resonance concept of the low-threshold field emission // Electronics. 2015. Vol. 4. No. 4. Pp. 1101–1108.

9. **Давидович М. В., Яфаров Р. К.** Импульсные и статические автоэмиссионные ВАХ углеродных нанокластерных структур: эксперимент и его интерпретация // Журнал технической физики. 2019. Т. 89. № 8. С. 1282–1293.

10. **Kleshch V. I., Porshyn V., Lützenkirchen-Hecht D., Obraztsov A. N.** Coulomb blockade and quantum confinement in field electron emission from heterostructured nanotips // Physical Review B. 2020. Vol. 102. No. 23. P. 235437.

11. **Bergfield J. P., Solis M. A., Stafford C. A.** Giant thermoelectric effect from transmission supernodes // ACS (American Chemical Society) Nano. 2010. Vol. 4. No. 9. Pp. 5314–5320.

12. **Dubi Y., Di Ventra M.** Colloquium: Heat flow and thermoelectricity in atomic and molecular junctions // Reviews of Modern Physics. 2011. Vol. 83. No. 1. Pp. 131–155.

13. **Karlstrцm O., Linke H., Karlstrцm G., Wacker A.** Increasing thermoelectric performance using coherent transport // Physical Review B. 2011. Vol. 84. No. 11. P. 113415.

14. **Sadeghi H.** Quantum and phonon interference-enhanced molecular-scale thermoelectricity // The Journal of Physical Chemistry C. 2019. Vol. 123. No. 20. Pp. 12556–12562.

15. **Andronov A., Budylina E., Shkitun P., Gabdullin P., Gnuchev N., Kvashenkina O., Arkhipov A.** Characterization of thin carbon films capable of low-field electron emission // Journal of Vacuum Science & Technology B. 2018. Vol. 36. No. 2. P. 02C108.

16. **Gabdullin P., Zhurkin A., Osipov V., Besedina N., Kvashenkina O., Arkhipov A**. Thin carbon films: Correlation between morphology and field-emission capability // Diamond & Related Materials. 2020. Vol. 105. May. P. 107805.

17. **Бизяев И. С., Габдуллин П. Г., Гнучев Н. М., Архипов А. В.** Низкопороговая полевая эмиссия электронов тонкими пленками металлов // Научно-технические ведомости СПбГПУ. Физико-математические науки. 2021. Т. 1 № .14. С. 127–111.

18. **Bizyaev I., Gabdullin P., Chumak M., Babyuk V., Davydov S., Osipov V., Kuznetsov A., Kvashenkina O., Arkhipov A.** Low-field electron emission capability of thin films on flat silicon substrates: Experiments with Mo and general model for refractory metals and carbon // Nanomaterials. 2021. Vol. 11. No. 12. P. 3350.

19. **Thompson C. V.** Solid-state dewetting of thin films // Annual Review of Materials Research. 2012. Vol. 42. No. 1. Pp. 399–434.

20. **Ruffino F., Grimaldi G.** Controlled dewetting as fabrication and patterning strategy for metal nanostructures // Physica Status Solidi A. 2015. Vol. 212. No. 8. Pp. 1662–1684.

21. **Niekiel F., Schweizer P., Kraschewski S. M., Butz B., Spiecker E.** The process of solid-state dewetting of Au thin films studied by in situ scanning transmission electron microscopy // Acta Materialia. 2015. Vol. 90. 15 May. Pp. 118–132.

22. **Kovalenko O., Szaby S., Klinger L., Rabkin E.** Solid state dewetting of polycrystalline Mo film on sapphire // Acta Materialia. 2017. Vol. 139. 15 October. Pp. 51–61.

23. **Weil K. S., Mast E. S., Sprenkle V. L.** Agglomeration behavior of solid nickel on polycrystalline barium titanate // Materials Letters. 2007. Vol. 61. No. 28. Pp. 4993–4996.

24. **Alburquenque D., Del Canto M., Arenas C., Tejo F., Pereira A., Escrig J.** Dewetting of Ni thin films obtained by atomic layer deposition due to the thermal reduction process: Variation of the thicknesses // Thin Solid Films. 2017. Vol. 638. 30 September. Pp. 114–118.

25. **Трофимович К. Р., Габдуллин П. Г., Архипов А. В.** Экспериментальная установка для исследования особенностей термоэлектрического эффекта в наноструктурах // Научно-технические ведомости СПбГПУ. Физико-математические науки. 2023. Т. 16. № 4. С. 101–117.

26. **Arkhipov A. V., Eidelman E. D., Zhurkin A. M., Osipov V. S., Gabdullin P. G.** Low-field electron emission from carbon cluster films: Combined thermoelectric/hot-electron model of the phenomenon // Fullerenes, Nanotubes and Carbon Nanostructures. 2020. Vol. 28. No. 4. Pp. 286–294.

27. **Arkhipov A., Trofimovich K., Arkhipov N., Gabdullin P**. Phonon drag contribution to thermopower for a heated metal nanoisland on a semiconductor substrate // Nanomaterials. 2024. Vol. 14. No. 20. P. 1684.

28. **Бизяев И. С., Карасев П. А., Карабешкин К. В., Габдуллин П. Г., Архипов А. В.** Трансформация структуры тонких металлических пленок при активировании их способности к низковольтной эмиссии электронов // Научно-технические ведомости СПбГПУ. Физико-математические науки. 2024. Т. 17. № 2. С. 80–93.

29. **Fedorovich R. D., Naumovets A. G., Tomchuk P. M.** Electron and light emission from island metal films and generation of hot electrons in nanoparticles // Physics Reports. 2000. Vol. 328. No. 2–3. Pp. 73–179.

30. **Weber L., Lehr M., Gmelin E.** Reduction of the thermopower in semiconducting point contacts // Physical Review B. 1992. Vol. 46. No. 15. Pp. 9511–9514.

31. **Barda H., Rabkin E.** Improving the thermal stability of nickel thin films on sapphire by a minor alloying addition of gold // Applied Surface Science. 2019. Vol. 484. 1 August. Pp. 1070–1079.

32. **Nsimama P. D., Herz A., Wang D., Schaaf P.** Influence of the substrate on the morphological evolution of gold thin films during solid-state dewetting // Applied Surface Science. 2016. Vol. 388. Pt. A. Pp. 475–482.

THE AUTHORS

NGUYEN Van Tu Ahn
Peter the Great St. Petersburg Polytechnic University
29 Politechnicheskaya St., St. Petersburg, 195251, Russia
anh.spbpu@gmail.com
ORCID: 0009-0004-7198-6329

GABDULLIN Pavel G.
Peter the Great St. Petersburg Polytechnic University
29 Politechnicheskaya St., St. Petersburg, 195251, Russia
pavel-gabdullin@yandex.ru
ORCID: 0000-0002-2519-2577

ARKHIPOV Alexander V.
Peter the Great St. Petersburg Polytechnic University
29 Politechnicheskaya St., St. Petersburg, 195251, Russia
arkhipov@rphf.spbstu.ru
ORCID: 0000-0002-3321-7797

СВЕДЕНИЯ ОБ АВТОРАХ

НГУЕН Ван Ту Ань – *аспирант* Высшей инженерно-физической школы Санкт-Петербургского политехнического университета Петра Великого.
195251, Россия, г. Санкт-Петербург, Политехническая ул., 29
anh.spbpu@gmail.com
ORCID: 0009-0004-7198-6329

ГАБДУЛЛИН Павел Гарифович – *кандидат физико-математических наук, доцент* Высшей инженерно-физической школы *Санкт-Петербургского политехнического университета Петра Великого.*
195251, Россия, г. Санкт-Петербург, Политехническая ул., 29
pavel-gabdullin@yandex.ru
ORCID: 0000-0002-2519-2577

АРХИПОВ Александр Викторович – *доктор физико-математических наук, профессор Высшей инженерно-физической школы Санкт-Петербургского политехнического университета Петра Великого.*

195251, Россия, г. Санкт-Петербург, Политехническая ул., 29

arkhipov@rphf.spbstu.ru

ORCID: 0000-0002-3321-7797

Received 09.02.2025. Approved after reviewing 19.05.2025. Accepted 19.05.2025.

Статья поступила в редакцию 09.02.2025. Одобрена после рецензирования 19.05.2025. Принята 19.05.2025.